Electron Emission at Locked Phases from the Laser-Driven Surface Plasma Wave

Ye Tian,[1] Jiansheng Liu,[1,*] Wentao Wang,[1] Cheng Wang,[1] Aihua Deng,[1] Changquan Xia,[1] Wentao Li,[1] Lihua Cao,[2]
Haiyang Lu,[1] Hui Zhang,[1] Yi Xu,[1] Yuxin Leng,[1] Ruxin Li,[1,†] and Zhizhan Xu[1,‡]

[1]*State Key Laboratory of High Field Laser Physics, Shanghai Institute of Optics and Fine Mechanics,
Chinese Academy of Sciences, Shanghai 201800, China*
[2]*Institute of Applied Physics and Computational Mathematics, Beijing 100088, China*

By irradiating a flat Al target with femtosecond laser pulses at moderate intensities of $\sim 10^{17}$ W/cm^2, we obtained stable collimated quasimonoenergetic electrons in the specular direction but deviated somewhat toward the target normal. An associated local minimum located on the other side of the specular direction seems to indicate that the peak actually results from the deflection of the collimated electrons from their initial ejection direction. We have proposed a two-step model in which some laser-accelerated electrons are able to leave the plasma in a narrow phase-locked window of the moving wave interference pattern, and are then steered toward the target normal by the ponderomotive force of the interference field. The periodic repetition of the electron emission leads to a pulse train of collimated quasimonoenergetic electrons with subcycle duration.

Collimated relativistic electron beams (*e* beams) with a narrow energy spread can find applications in ultrafast electron diffraction, fast ignition, and tabletop electron accelerators provided that flux and duty cycles are sufficiently high [1–3]. Compared to the electron gun, the *e* beams produced by femtosecond laser pulses inherit the ultrafast characteristic with a duration down to a femtosecond time scale, which opens a way for ultrafast electron diagnostics [4–6]. Laser-driven quasimonoenergetic *e* beams have been produced by the wakefield acceleration mechanism operating in the so-called "blowout" mode [7,8]. However, in this method the quasimonoenergetic *e* beams are produced with energies of several tens of MeV, which is too high for many applications.

Most experiments on fast electron generation from the laser-solid interaction indicate that the emitted *e* beams exhibit broad-cone emission with broad energy spectra, and are ejected at angles between the target normal and specular directions with poor controllability [9–14]. Only a few groups have observed highly directed electron emission from the laser-solid interactions by selecting appropriate laser intensities [9,10], the target material such as SiO$_2$, and the plasma scale length [11]. The "jetlike" collimated *e* beams with the Maxwellian energy spectrum was first observed along the specular direction by focusing a high-contrast-ratio laser pulse at 4×10^{16} W/cm^2 onto a solid SiO$_2$ target [9], where a very steep gradient scale length was obtained. Similar results have recently been reproduced from SiO$_2$ targets by Mordovanakis *et al.* [11] via adjusting the plasma scale length and from Al targets by Wang *et al.* [10]. Besides the collimated *e* beam, an associated local minimum close to the specular direction implies that the collimated *e* beam is deflected outward by the ponderomotive force of the laser beam [11]. However,

the deflection of the collimated *e* beam toward the target normal should have some theoretical justifications. The underlying physics of the electron ejection from the solid targets is still elusive, which renders the manipulation of the collimated *e* beam emission unavailable.

In this Letter, we demonstrate stable collimated quasimonoenergetic *e* beam generation close to the specular direction that was obtained by irradiating a flat Al target with femtosecond laser pulses at moderate intensities. We propose a simple two-step model to characterize the underlying physics behind the deflection of ejected electrons. In the first step, we believe that some accelerated electrons more or less along the specular direction are ejected from the laser-driven surface plasma wave but only periodically at a specific phase of the laser field pattern. At the second step, these electrons are steered slightly outward toward the target normal by the ponderomotive force of the combined field of the incident laser and its coherent reflection, which we term simply the interference field. An energy loss due to deflection in the interference field predicted by this model is confirmed experimentally.

The experiments were carried out with a Ti:sapphire femtosecond laser, which delivered laser pulses with energy up to 31 mJ and a duration of 65 fs on the target surface. A *p*-polarized laser beam was focused by an $f/4$ off-axis parabola onto a flat aluminum target with an angle of incidence θ, as shown in Fig. 1. The diameter of the focal spot is 8 μm at the full width at half maximum (FWHM), containing about 40% of laser energy. The laser intensity contrast ratio was measured to be better than 10^8 at 50 ps and 10^7 at 10 ps before the peak of the main pulse [15]. The spatial angular distribution of emitted electrons was recorded in the single-shot operation mode by an imaging plate (Fujifilm BAS-SR2025) [16], which was
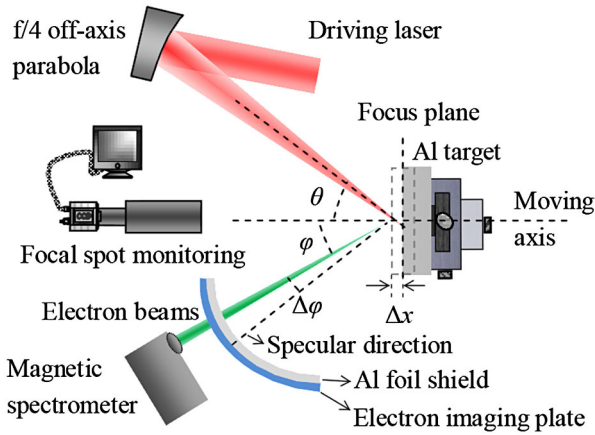
FIG. 1 (color online).   Schematic diagram of the experimental
setup for detecting electron emission.

bent to become a circular cylinder with its axis fixed at the
focus and perpendicular to the incident plane of laser. The
imaging plate was covered with a 17 μm thick Al foil in
order to prevent low energy x-ray, scattering light. A 0.1-T
dipolar magnet was installed to measure the energy spectra
of the emitted electrons at some specialized directions.

Figures 2(a)–2(d) show the single-shot spatial angular
distributions of emitted electrons from an Al target at
$\theta = 45°$ with different offsets of Δx. When the target
was moved away from the focus along the target normal
with $\Delta x = 0/120/240/360$ μm, the corresponding laser
intensities on the target, which were estimated from the

laser energy, pulse duration, and the spot size, were
$3/2/1.1/0.6 \times 10^{17}$ W/cm^2, respectively. Assuming the
plasma expands isothermally [17], the scale length was
estimated, varying between $\sim 0.1\lambda$ and 0.5λ. As shown
in Fig. 2(a), when the focus was on the target surface
($\Delta x = 0$), a collimated e beam centered at the direction
of $\varphi = 38°$ was obtained with a divergence angle of
146 mrad (8.3°, FWHM) in the incident plane and a charge
of ~ 9 pC within the FWHM spatial zone. As the target
was moved forward with $\Delta x = 120/240/360$ μm, the
angular distributions exhibited the jetlike collimated e
beams [Figs. 2(b)–2(d)]. The divergence angles and the
total charges of the collimated e beams were measured to
be 52/37/26 mrad and 3 pC/250 fC/60 fC, respectively.
The emission angles were slightly deflected to the target
normal at $\varphi = 41°/42°/43.5°$. A local minimum was
located close to the specular direction but on the opposite
side. While placing the imaging plate closer to the focus
with a distance of 6 cm to measure the ejected electrons at
$\Delta x = 120$ μm, the collimated e beams, which exhibit a
spatial modulation and the associated local minimum, are
obviously located on the opposite sides of the specular
direction as shown in Fig. 2(e).

By changing the laser incidence angle θ from 34° to 82°
with the target surface set at $\Delta x = 120$ μm, we measured
the angular distributions of the ejected electrons, as shown
in Figs. 2(f)–2(h) and to be compared with Fig. 2(b). The
divergences, deflection angles $\Delta\varphi$, and total charges of
the collimated e beams were 65/42/38 mrad, $-2.2°/$
$-3°/-5°$, and 0.9 pC/5.3 pC/4.3 pC, respectively.

In addition, single-shot electron spectra of the collimated
e beams were measured at the emission angle ($\varphi = 42°$)
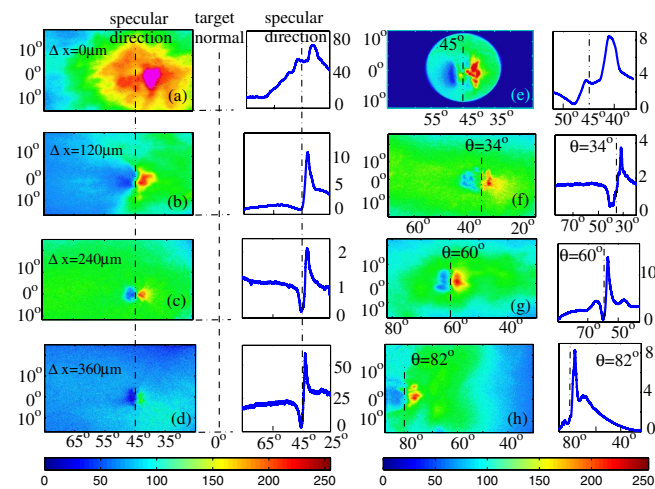with $\Delta x = 240$ μm and $\theta = 45°$ as shown in Fig. 3.

FIG. 2 (color online).   Single-shot images and corresponding
lineouts along the angular distributions. The lineouts are inte-
grated spatially within $\pm 5°$ along the vertical axis (blue lines).
(a)–(d) Corresponding to different focal positions with
$\Delta x = 0, 120, 240, 360$ μm, respectively. Dashed lines show the
specular direction at 45° and the target normal at 0°. (e) The
imaging plate covered with a circular aperture of 3 cm diameter
was placed at 6 cm away from the focus to calibrate the specular
direction and measure the fine structure. (f)–(h) Corresponding to
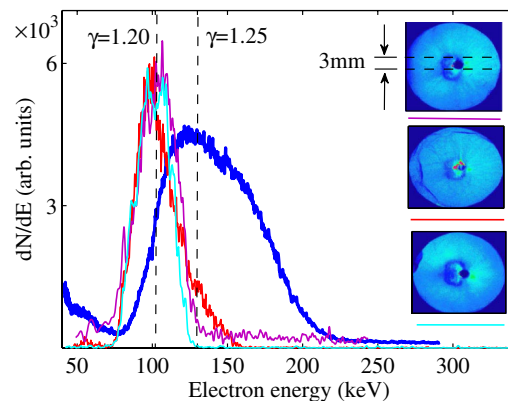different angles of incidence at 34°, 60°, 82°, respectively.

FIG. 3 (color online).   Three shot-to-shot energy spectra of
the collimated e beams measured at $\varphi = 42°$, and the spectra
of the peripheral electrons measured at $\varphi = 35°$ (blue line). An
aperture with a diameter of 3-mm covered by an imaging plate
with a hole was placed at the entrance of the magnet to pick out
the collimated e beams as well as to monitor the selection as
shown in the insets. The 3 images correspond to the 3 displayed
spectra of the collimated e beams. The offset $\Delta x = 240$ μm and
the angle of incidence was 45°.

The entrance of the magnet was placed at 10 cm away from the focus, and an aperture of 3 mm in diameter was placed at the entrance to pick out the collimated e beams. An imaging plate with a same-size hole was placed before the aperture to monitor whether the collimated e beams enter the magnet as shown in the insets of Fig. 3. The shot-to-shot energy spectra of the collimated e beams exhibited a quasimonoenergetic distribution with peak energy of ~ 100 keV, a FWHM energy spread of $\sim 30\%$, and good reproducibility. The energy spectrum of the peripheral electrons around the collimated e beams, for example, at $\varphi \sim 35°$ in the incident plane, was also measured [Fig. 3 ($\gamma = 1.25$)]. It exhibited a broader distribution with a higher peak energy of ~ 130 keV.

The expulsion of the e beam by the ponderomotive force of the laser beam could not explain why the collimated e beam was necessarily deflected to the target normal if the origin of the electron emission was not considered, and, in particular, at what phase the ejection into the reflection field occurred. The physical picture of ejecting electrons from near the plasma surface more or less along the specular direction can be approached by two dimensional (2D) particle-in-cell (PIC) simulations with results such as the time frame set shown in Fig. 4, from the case where a 65 fs p-polarized laser pulse with 1×10^{17} W/cm^2($a_0 = 0.3$) intensity is focused with $\omega_0 = 5\lambda$ at a $45°$ angle of incidence. The plasma-density profile is assumed as an exponential profile from $0.1n_c$ to $16n_c$ with a scale length
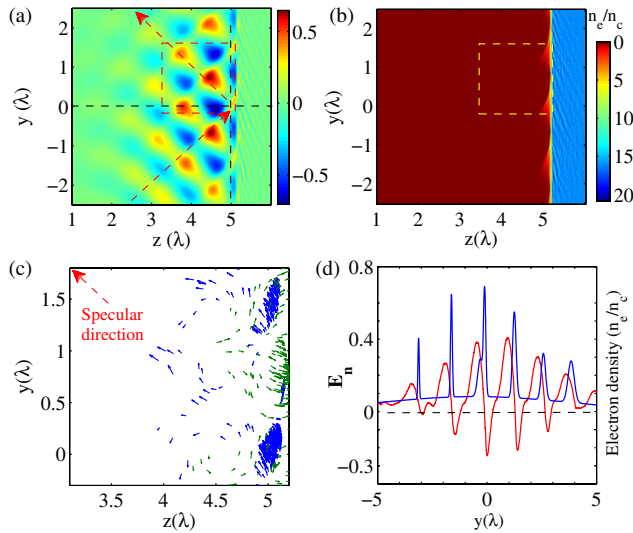

FIG. 4 (color online). (a) Spatial distribution of longitudinal electric field amplitude $\mathbf{E}_n$ and (b) the normalized electron density at the peak laser intensity. (c) Momentum distribution of electrons within a spatial period [corresponding to the yellow rectangle zone in (b)] along the surface. The dense left-and-upward going arrows near $z = 4.9\lambda$ and $y = 0\lambda$ indicate that the laser-accelerated electrons move outward more or less near the specular direction and form the wave crest. (d) Spatial distributions of the electric field amplitude E_n (red line) and electron density (blue line) at the wave crest ($z = 4.9\lambda$) along the surface direction.

of 0.2λ. Figures 4(a) and 4(b) show the time frame set of spatial distributions of the laser electric field $\mathbf{E}_n$ (the vector component of the interference field along the target normal) and the normalized electron density n_e/n_c at the peak of the laser pulse interaction with the target. The interference field is built up in the triangular overlap region of the incident and scattered light beams, and the surface plasma wave is produced, which has a spatial period of $\lambda/\cos45°$ and propagates along the surface at the superluminous phase velocity of $c/\cos45°$. Unlike the oscillating mirror models [18,19], but like the coherent wave emission models [20–22], electrons transiting the subcritical density region outside the steep plasma-density cliff are accelerated near $z = 5\lambda$ in Fig. 4(c), (this is step 1 of the process we are discussing) by complicated and nonuniform fields whose effects are not yet well analyzed [23]. For the moment it seems that the electrons probably escape with some significant momentum parallel to the surface. Given that the plasma wave is moving parallel to the surface faster than light, it is clear that in this sense the electrons cannot be really trapped in the surface direction, so there is as yet no obvious applicable formalism with which to estimate what velocity the escaping electrons can begin their voyage along with the reflected laser field.

Figure 4(c) shows the momentum distribution of electrons within two spatial periods near $y = 0\lambda$ along the surface. The dense left-and-upward going arrows near $z = 4.9\lambda$ and $y = 0\lambda$ indicate that the laser-accelerated electrons move outward more or less near the specular direction and form the wave crest, which corresponds to the density spike as shown in Fig. 4(d). The maximum kinetic energy of outgoing electrons is about 160 keV. However, at the wave trough ($y = -0.7\lambda$) electrons are pushed back into the plasma with the maximum momentum. This is precisely the phenomenon investigated by others [20–25] that produces the peaks in the current giving rise to the high harmonics observed. We can easily discern that a small amount of electrons escape away from the plasma wave more or less along the specular direction as shown in the left vacuum region of Fig. 4(c). Electron emissions along the specular direction and target normal have been previously reported [26–29]. Figure 4(d) shows the spatial periodical distribution of the electric field $\mathbf{E}_n$ and normalized electron density at the wave crest ($z = 4.9\lambda$) along the surface direction. The peak electron density at the wave crest appears periodically at the fixed phases when the electric field $\mathbf{E}_n$ changes the sign from the positive to the negative, from which we can infer that the electrons which actually escape are those which arrive at a favorable phase at the top of their near-escape orbits and then take a second step to freedom.

Now we believe that some of these accelerated electrons at the wave crests a $\lambda/\cos\theta$ apart are the ones which escape in a manner that has yet to be determined (what we have called "the second step"), but at the moment there

is no clear indication as to the value of the escape momentum or of its direction. This information might be obtained in future work by tracing the trajectories of particular selected electrons in the PIC simulations, as suggested by Gibbon [23]. In the meantime, to see what can happen we will examine a simple toy model, assuming the character of typical escaping electrons and using the vacuum form for the electromagnetic fields not too close to the target surface.

Supposing an ejected electron escaping away from the plasma wave [Fig. 5(a)], its trajectory thereafter will abide by the motion of a free electron in the interference field and be governed by relativistic Lorentz equations [30]. The interference field can be described by the superposition of two laser fields which propagate orthogonally along $-x$ and z directions, respectively, and have a spatiotemporal Gaussian profile. The vector potential is described as $\vec{a} = \vec{a}_i(t + x, y, z) + \vec{a}_r(t - z, x, y)$, $\vec{a}_i$ and $\vec{a}_r$ are presented as follows for the p polarization:

$$\vec{a}_i(t + x, y, z) = a_{i0} \frac{\omega_0}{\omega(x)} \exp\left(-\frac{(t + x)^2}{T^2} - \frac{y^2 + z^2}{\omega(x)^2}\right)$$
$$\times \cos(t + x - \varphi_{Ri} - \varphi_{Gi})\hat{z}, \quad (1)$$

$$\vec{a}_r(t - z, x, y) = \eta \times a_{i0} \frac{\omega_0}{\omega(z)} \exp\left(-\frac{(t - z)^2}{T^2} - \frac{x^2 + y^2}{\omega(z)^2}\right)$$
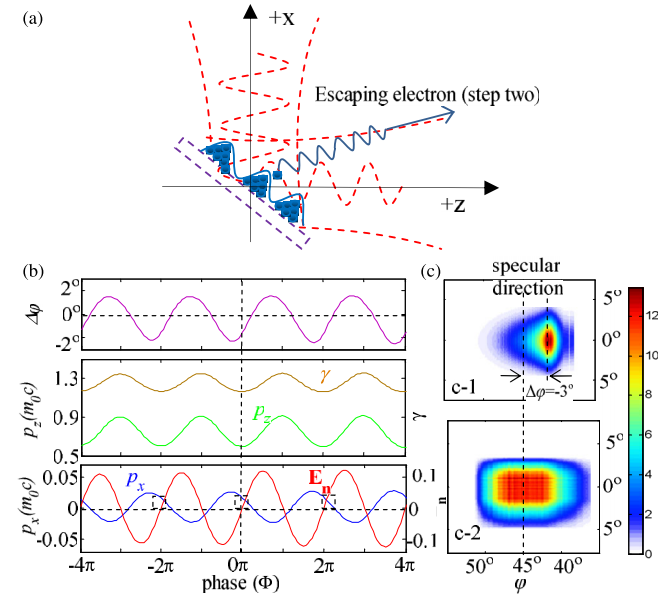$$\times \cos(t - z - \varphi_{Rr} + \varphi_{Gr})\hat{x}. \quad (2)$$

FIG. 5 (color online). (a) Schematic geometry of electron motion in an interference field in the incident plane. (b) The final electron momentum p_z, p_x (blue line), energy γ, $\Delta\varphi = \tan^{-1} p_x/p_z$ (top) and the initial superposition field $\mathbf{E}_n$ (red line) when the electron escapes from the surface plasma wave. (c) The statistic angular distributions of electrons escaping from the surface plasma wave at different initial phases: (c-1) $\Phi_i = 2N\pi$ [rectangle zone in (b)] and (c-2) Φ_i from 0 to 2π.

Where a_{i0} is the peak amplitude at the focus normalized by mc^2/e, the beam waist at focus is ω_0, and at arbitrary z is $\omega(z) = \omega_0\sqrt{1 + (z/z_r)^2}$, $z_r = \omega_0^2/2$ is the Rayleigh length, and T corresponds to the pulse duration. $\varphi_{Ri} = (y^2 + z^2)/R(x)^2$ and $\varphi_{Rr} = (x^2 + y^2)/R(z)^2$ are the phases associated with the curvatures of the incident and reflected wave fronts, and the radius $R(x) = x + x_r^2/x$, $R(z) = z + z_r^2/z$. $\varphi_{Gi} = \tan^{-1}(x/z_r)$ and $\varphi_{Gr} = \tan^{-1}(z/z_r)$ are the Guoy phases, η is the reflection efficient, and a phase jump π was assumed for the reflected laser field. The laser parameters are as follows: spot size $\omega_0 = 5\lambda$, pulse width $T = 20T_0$ (T_0 is the laser oscillation period). The incident and reflected laser intensity are $a_{i0} = 0.35$ and $a_{r0} = 0.25(\eta \sim 70\%)$, respectively. The focal planes of the two laser beams are set at $x = -150\lambda$ and $z = 150\lambda$, respectively.

The electron escaping away from the plasma surface is initially located in the plane of $z = -x$ and its initial velocity along the $+z$ direction is assumed as $0.6c$ ($\gamma = 1.25$, and $p_z = 0.75$). Without loss of generality, setting the initial position of the electron at $z = 2\lambda$, we calculate the final momentum p_z, p_x that the electron obtains from the interference field by scanning the initial instant t_i, at which the electron escapes away from the surface. The final momentum is obtained by calculating the electron's relativistic dynamics over a long time until the field seen by the electron becomes negligible. Figure 5(b) shows the final momentum p_z, p_x and energy γ when t_i is scanned from $-2T_0$ to $2T_0$ (corresponding to the initial phase Φ_i from -4π to 4π). Owing to repulsion of the ponderomotive force of the interference field, the electron may be steered both toward the target normal and surface directions with a deflection angle $\Delta\varphi = -\tan^{-1}(p_x/p_z)$ if the electron is captured at arbitary phases relative to the laser field [Fig. 5(b) (top)]. This inconsistency with the measured collimated e beam deflected only toward the target normal implies that electrons are ejected from the plasma wave at phases locked to the laser wave pattern. Considering that the electrons are ejected initially in a range of directions, for example, with a uniform distribution within $\pm 5°$ centered at the sepcular direction, the final statistic angular distribution of the ejected electrons captured at the phases $\Phi = 2N\pi(N = 0, \pm 1, \ldots)$ is calculated and shown in Fig. 5(c) [panel (c-1)]. The electrons are shifted to the target normal with $\Delta\varphi = -3°$, which reproduces the deflection effect as demonstrated in Fig. 2. Additionally, the collimated e beam obtains an energy loss of $\Delta E \sim -35$ keV from the interference field as the change of γ shows, which can explain the measured energy loss as compared with the energy of the peripheral electrons (Fig. 3). If assuming the electrons were ejected initially at arbitrary phases from 0 to 2π, the statistic angular distribution is plotted as shown in Fig. 5(c) [panel (c-2)], which presents a broadening angular distribution. In this case, some electrons will gain and others will lose energy; therefore, the energy spectrum of the electrons will also be broadened. This result indicates that the

observed electrons at other directions except the collimated *e* beams are ejected away from the plasma wave at arbitrary phases.

The variation of the deflection angle as the target surface is moved along the target normal can be attributed to the intensity variation of the interference field on the target surface. So this toy model, simple but illustrative, can explain the deflection of the collimated *e* beam and the energy loss very well.

In conclusion, we have demonstrated for our system the experimental robustness of the phenomenon of collimated quasimonoenergetic *e* beams and their deflection, as obtained from irradiation of a flat Al target with a short pulse at moderate intensities. By proposing a two-step model we reveal that in each cycle of the laser oscillation, some electrons at a favorable phase at the top of their near-escape orbits escape away from the plasma wave more or less along the specular direction. They are acted on by the interference field at the locked phases and inevitably steered slightly to the target normal. The periodic repetition of the electron emission, every optical cycle, leads to a pulse train of collimated *e* beams with subcycle duration. Since the repulsion effect of the ponderomotive force of the interference field always exists, the issue on the phase of electron emission from the laser-solid interaction, which has never been addressed before, should be inspected extensively in a much broader range of laser parameters.

---

*michaeljs_liu@siom.ac.cn
†ruxinli@mail.shcnc.ac.cn
‡zzxu@mail.shcnc.ac.cn

[1] S. Tokita, M. Hashida, S. Inoue, T. Nishoji, K. Otani, and S. Sakabe, Phys. Rev. Lett. **105**, 215004 (2010).
[2] M. Tabak, J. Hammer, M. E. Glinsky, W. L. Kruer, S. C. Wilks, J. Woodworth, E. M. Campbell, M. D. Perry, and R. J. Mason, Phys. Plasmas **1**, 1626 (1994).
[3] J. S. Liu et al., Phys. Rev. Lett. **107**, 035001 (2011).
[4] B. J. Siwick, J. R. Dwyer, R. E. Jordan, and R. J. Dwayne Miller, Science **302**, 1382 (2003).
[5] A. H. Zewail, Annu. Rev. Phys. Chem. **57**, 65 (2006).
[6] S. Tokita, S. Inoue, S. Masuno, M. Hashida, and S. Sakabe, Appl. Phys. Lett. **95**, 111911 (2009).
[7] J. Faure, Y. Glinec, A. Pukhov, S. Kiselev, S. Gordienko, E. Lefebvre, J.-P. Rousseau, F. Burgy, and V. Malka, Nature (London) **431**, 541 (2004).
[8] S. Mangles et al., Nature (London) **431**, 535 (2004).
[9] S. Bastiani, A. Rousse, J. P. Geindre, P. Audebert, C. Quoix, G. Hamoniaux, A. Antonetti, and J.-C. Gauthier, Phys. Rev. E **56**, 7179 (1997).
[10] W. T. Wang, J. Liu, Y. Cai, C. Wang, L. Liu, C. Xia, A. Deng, Y. Xu, Y. Leng, R. Li, and Z. Xu, Phys. Plasmas **17**, 023108 (2010).
[11] A. G. Mordovanakis et al., Phys. Rev. Lett.**103**, 235001 (2009).
[12] F. Brandl, B. Hidding, J. Osterholz, D. Hemmers, A. Karmakar, A. Pukhov, and G. Pretzler, Phys. Rev. Lett. **102**, 195001 (2009).
[13] D. F. Cai, Y. Q. Gu, Z. J. Zheng, T. S. Wen, S. T. Chunyu, Z. B. Wang, and X. D. Yang, Phys. Plasmas **10**, 3265 (2003).
[14] Z. M. Sheng, Y. Sentoku, K. Mima, J. Zhang, W. Yu, and J. Meyer-ter-Vehn, Phys. Rev. Lett. **85**, 5340 (2000).
[15] Yi Xu, Y. X. Leng, L. H. Lin, W. Y. Wang, Y. S. Huang, R. X. Li, and Z. Z. Xu, Chin. Optic. Lett. **8**, 123 (2010).
[16] K. A. Tanaka T. Yabuuchi, T. Sato, R. Kodama, Y. Kitagawa, T. Takahashi, T. Ikeda, Y. Honda, and S. Okuda, Rev. Sci. Instrum. **76**, 013507 (2005).
[17] W. L. Kruer, *The Physics of Laser Plasma Interactions* (Addison-Wesley, Redwood City, 1988).
[18] S. V. Bulanov et al., Phys. Plasmas **1**, 745 (1994).
[19] S. Gordienko, A. Pukhov, O. Shorokhov, and T. Baeva, Phys. Rev. Lett. **93**, 115002 (2004).
[20] F. Quéré, C. Thaury, P. Monot, S. Dobosz, and Ph. Martin, Phys. Rev. Lett. **96**, 125004 (2006).
[21] C. Thaury et al., Nature Phys. **3**, 424 (2007).
[22] Antonin Borot, Arnaud Malvache, Xiaowei Chen, Aurélie Jullien, Jean-Paul Geindre, Patrick Audebert, Gérard Mourou, Fabien Quéré, and Rodrigo Lopez-Martens, Nature Phys. **8**, 416 (2012).
[23] P. Gibbon, Phys. Rev. Lett. **76**, 50 (1996).
[24] J. S. Liu, C. Xia, L Liu, R. Li, and Z. Xu, Laser Part. Beams **27**, 365 (2009).
[25] C. Thaury and F. Quéré, J. Phys. B **43**, 213001 (2010).
[26] Y. Sentoku et al., Phys. Plasmas **6**, 2855 (1999).
[27] R. Kodama, K. A. Tanaka, Y. Sentoku, T. Matsushita, K. Takahashi, H. Fujita, Y. Kitagawa, Y. Kato, T. Yamanaka, and K. Mima, Phys. Rev. Lett. **84**, 674 (2000).
[28] T. Johnston et al., Bull. Am. Phys. Soc. **53** (2008).
[29] H. Ruhl, Y. Sentoku, K. Mima, K. A. Tanaka, and R. Kodama, Phys. Rev. Lett. **82**, 743 (1999)
[30] Paul Gibbon, *Short Pulse Laser Interaction with Matter, an Introduction* (Imperial College Press, London, 2005).